All-optical NRZ wavelength conversion based on a single hybrid III-V/Si SOA and optical filtering

YINGCHEN WU,[1,2,*] QIANGSHENG HUANG,[1,2] SHAHRAM KEYVANINIA,[2] ANDREW KATUMBA,[2] JING ZHANG,[2] WEIQIANG XIE,[2] GEERT MORTHIER,[2] JIAN-JUN HE,[1] AND GUNTHER ROELKENS[2]

[1]State Key Laboratory of Modern Optical Instrumentation, College of Optical Science and Engineering, Zhejiang University, Hangzhou, 310027, China
[2]Photonics Research Group, INTEC, Ghent University—IMEC, Sint-Pietersnieuwstraat 41, 9000 Ghent, Belgium
*wuyingchen@ioe-zju.org

Abstract: We demonstrate all-optical wavelength conversion (AOWC) of non-return-to-zero (NRZ) signal based on cross-gain modulation in a single heterogeneously integrated III-V-on-silicon semiconductor optical amplifier (SOA) with an optical bandpass filter. The SOA is 500 μm long and consumes less than 250 mW electrical power. We experimentally demonstrate 12.5 Gb/s and 40 Gb/s AOWC for both wavelength up and down conversion.

References and links

1. S. J. B. Yoo, "Wavelength conversion technologies for WDM network applications," J. Lightwave Technol. **14**(6), 955–966 (1996).
2. P. Runge, C. A. Bunge, and K. Petermann, "All-optical wavelength conversion with extinction ratio improvement of 100 Gb/s RZ-signals in ultralong bulk semiconductor optical amplifiers," IEEE J. Quantum Electron. **46**(6), 937–944 (2010).
3. S. Yamashita, S. Y. Set, and D. Matsumoto, "Polarization-independent self-pumped wavelength converter using the four wave mixing in a semiconductor optical amplifier," in Proc. CLEO/Pacific Rim. **4**, 1163–1164 (1999).
4. G. Constestabile, N. Calabretta, M. Presi, and E. Ciaramella, "Single and multicast wavelength conversion at 40 Gb/s by means of fast nonlinear polarization switching in a SOA," IEEE Photonics Technol. Lett. **17**(12), 2652–2654 (2005).
5. J. Leuthold, D. M. Marom, S. Cabot, J. J. Jaques, R. Ryf, and C. R. Giles, "All-optical wavelength conversion using a pulse reformatting optical filter," J. Lightwave Technol. **22**(1), 186–192 (2004).
6. Y. Liu, E. Tangdiongga, Z. Li, H. de Waardt, A. M. J. Koonen, G. D. Khoe, and H. J. S. Dorren, "Error-free 320 Gb/s SOA-based wavelength conversion using optical filtering," in Proc. OFC, Paper PDP 28 (2005).
7. X. Yi, R. Yu, J. Kurumida, and S. J. B. Yoo, "A theoretical and experimental study on modulation-format-independent wavelength conversion," J. Lightwave Technol. **28**(4), 587–595 (2010).
8. G. T. Kanellos, N. Pleros, D. Pentrantonakis, P. Zakynthinos, H. Avramopoulos, G. Maxwell, and A. Poustie, "All-optical 3R burst-mode reception at 40 Gb/s using four integrated MZI switches," Opt. Express **15**(8), 5043–5049 (2007).
9. D. Apostolopoulos, K. Vyrsokinos, P. Zakynthinos, N. Pleros, and H. Avramopoulos, "An SOA-MZI NRZ wavelength conversion scheme with enhanced 2R regeneration characteristics," IEEE Photonics Technol. Lett. **21**(19), 1363–1365 (2009).
10. M. Hattori, K. Nishimura, R. Inohara, and M. Usami, "Bidirectional data injection operation of hybrid integrated SOA-MZI all-optical wavelength converter," J. Lightwave Technol. **25**(2), 512–519 (2007).
11. M. Spyropoulou, N. Pleros, K. Vyrsokinos, D. Apostolopoulos, M. Bougioukos, D. Petrantonakis, and H. Avramopoulos, "40 Gb/s NRZ wavelength conversion using a differentially-biased SOA-MZI: theory and experiment," J. Lightwave Technol. **29**(10), 1489–1499 (2011).
12. S. Keyvaninia, M. Muneeb, S. Stanković, P. J. Van Veldhoven, D. Van Thourhout, and G. Roelkens, "Ultra-thin DVS-BCB adhesive bonding of III-V wafers, dies and multiple dies to a patterned silicon-on-insulator substrate," Opt. Mater. Express **3**(1), 35–46 (2013).
13. A. W. Fang, H. Park, O. Cohen, R. Jones, M. J. Paniccia, and J. E. Bowers, "Electrically pumped hybrid AlGaInAs-silicon evanescent laser," Opt. Express **14**(20), 9203–9210 (2006).

14. H. Park, A. W. Fang, O. Cohen, R. Jones, M. J. Paniccia, and J. E. Bowers, "A hybrid AlGaInAs-Silicon Evanescent Amplifier," IEEE Photonics Technol. Lett. **19**(4), 230–232 (2007).
15. S. Cheung, Y. Kawakita, K. Shang, and S. J. Yoo, "Highly efficient chip-scale III-V/silicon hybrid optical amplifiers," Opt. Express **23**(17), 22431–22443 (2015).
16. S. Keyvaninia, G. Roelkens, D. Van Thourhout, J. M. Fedeli, S. Messaoudene, G. H. Duan, M. Lamponi, F. Lelarge, E. J. Geluk, and B. Smalbrugge, "A highly efficient electrically pumped optical amplifier integrated on a SOI waveguide circuit," in IEEE 9th International Conference on Group IV Photonics (GFP). 222–224 (2012).
17. A. Abbasi, J. Verbist, J. Van Kerrebrouck, F. Lelarge, G. H. Duan, X. Yin, J. Bauwelinck, G. Roelkens, and G. Morthier, "28 Gb/s direct modulation heterogeneously integrated C-band InP/SOI DFB laser," Opt. Express **23**(20), 26479–26485 (2015).
18. S. Keyvaninia, S. Verstuyft, L. Van Landschoot, F. Lelarge, G.-H. Duan, S. Messaoudene, J. M. Fedeli, T. De Vries, B. Smalbrugge, E. J. Geluk, J. Bolk, M. Smit, G. Morthier, D. Van Thourhout, and G. Roelkens, "Heterogeneously integrated III-V/silicon distributed feedback lasers," Opt. Lett. **38**(24), 5434–5437 (2013).
19. Q. Huang, J. Cheng, L. Liu, Y. Tang, and S. He, "Ultracompact tapered coupler for the Si/III-V heterogeneous integration," Appl. Opt. **54**(14), 4327–4332 (2015).
20. M. Lamponi, S. Keyvaninia, C. Jany, F. Poingt, F. Lelarge, G. de Valicourt, G. Roelkens, D. Van Thourhout, S. Messaoudene, J.-M. Fedeli, and G. H. Duan, "Low-threshold heterogeneously integrated InP/SOI lasers with a double adiabatic taper coupler," IEEE Photonics Technol. Lett. **24**(1), 76–78 (2012).
21. J. Dong, X. Zhang, S. Fu, J. Xu, P. Shum, and D. Huang, "Ultrafast all-optical signal processing based on single semiconductor optical amplifier and optical filtering," IEEE J. Sel. Top. Quantum Electron. **14**(3), 770–778 (2008).
22. D. Nesset, T. Kelly, and D. Marcenac, "All-optical wavelength conversion using SOA nonlinearities," IEEE Commun. Mag. **36**(12), 56–61 (1998).

1. Introduction

The rapid growth of the internet and internet-related services call for large-capacity and high-speed data networking. All-optical networking allows for data reconfiguration directly in the optical layer rather than in the electronic layer. Since no optical-to-electrical-to-optical (OEO) data conversions are involved, power consumption and bandwidth of such communication networks can be substantially improved. An important function that needs to be implemented for all-optical networks is all-optical wavelength conversion (AOWC). For example, in wavelength division multiplexed (WDM) networks AOWC can remove wavelength blocking in optical cross connects [1].

AOWC based on semiconductor optical amplifiers (SOA) has a number of advantages, including high-speed operation and easy integration with other optoelectronic and passive waveguide components. Many SOA-based AOWC techniques on the InP platform have been reported, achieving data rates up to 320 Gb/s [2–6], based on cross-gain modulation (XGM), cross-phase modulation (XPM) or four wave mixing (FWM). 2R/3R regeneration and the wavelength conversion of advanced modulation format signals have also been realized using SOA-based Mach-Zehnder interferometric structures [7, 8]. Most experiments are carried out using a Return-to-Zero (RZ) data format, while the Non-Return-to-Zero (NRZ) data format is still the dominant one in commercial optical networks. AOWC for NRZ signals has been reported by means of an SOA-MZI based push-pull structure [9], bidirectional driving schemes [10] or a differentially-biased scheme [11].

Recently, silicon photonics is emerging as a new promising platform for photonic integrated circuits, because of its compatibility with CMOS fabrication technology and the fact that the large refractive index contrast allows for densely integrated photonic circuits. However, silicon is an indirect bandgap material, which cannot be used for SOAs and lasers. Through adhesive bonding technology [12] and molecular bonding technology [13], one can heterogeneously integrate III-V materials, to realize SOAs [14–16] and lasers [13, 17, 18] on the silicon photonics platform. The SOAs in such a hybrid III-V/silicon platform [14–16] show large gain and small footprint, which makes it attractive to realize AOWC in a compact form factor and with low power consumption.

In this paper, we demonstrate AOWC of 12.5 Gb/s NRZ data based on cross-gain modulation in an SOA heterogeneously integrated on an SOI waveguide circuit with an optical bandpass filter (OBF) slightly blue shifted to improve the amplitude recovery and eliminate the pattern effect. The SOA is only 500 μm long and the driving current is 85 mA

(at a bias voltage of 2.85 V) resulting in a power consumption below 250 mW. The average optical signal input power is as low as −6.5dBm while the input power of the CW probe light is 0.5 dBm. With optical data and continuous-wave (CW) probe light coupled into the SOA through grating couplers in counter-propagating directions, 12.5 Gb/s AOWC is achieved in both wavelength-up and wavelength-down conversion scenarios. Error-free operation (BER 10^{-9}) is obtained. We also study AOWC of 40 Gb/s NRZ data. A power penalty less than 3 dB at a bit error rate below 10^{-5} is obtained in this case.

2. Concept

Figure 1 shows the schematic diagram of the SOA, a cross section of taper tip, as well as the mode transformation structure to couple light to and from the silicon waveguide. The III-V gain section is integrated on top of the silicon-on-insulator waveguide circuit by means of adhesive bonding using DVS-BCB [16]. The silicon waveguide layer in taper area comprises both 400-nm-thick and 220- nm-thick silicon waveguides, which has better process tolerance than 220-nm-only taper as described in Ref [19]. 400-nm-thick silicon adiabatic taper structures can offer a robust high-efficient mode coupling between silicon waveguide and III-V waveguide with a high confinement factor in quantum well region. The details of design and fabrication process can be found in [18, 20]. There are two taper sections in the tapered III-V waveguide. In the first taper section, the taper length is 30 μm, the mesa width reduces from 3 μm to 0.9 μm. In the second taper section, the taper length is 100 μm and the mesa width reduces to 400 nm. Meanwhile, the tapered SOI waveguide in this section is tapered from 300 nm to 1 μm. This taper structure has been successfully implemented for a hybrid SOA [16]. The III-V epitaxial layer stack consists of a 200 nm thick n-InP contact layer, two 100 nm thick InGaAsP separate confinement heterostructure layers (bandgap wavelength 1.17 μm), six InGaAsP quantum wells (6 nm thick, emission wavelength 1.55 μm) surrounded by InGaAsP barriers, a 1.5 μm thick p-InP top cladding, and a 100 nm p + + InGaAs contact layer. The III-V mesa structure is fabricated by wet etching, resulting in a V-shaped mesa that allows for both high confinement factor and sharp taper tips. After propagating through the taper area, the optical mode is predominantly confined in the III-V active layer. The current design produces a relatively large confinement factor of 12% in the quantum wells. For SOAs that works in saturation for wavelength conversion, with a given active length and injected current, a large confinement factor results in a relatively low saturation power, short gain recovery time and a large cross gain modulation.
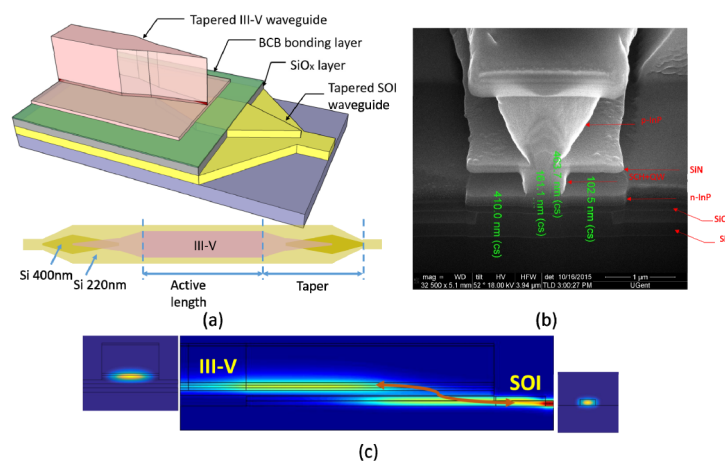

Fig. 1. (a) Schematic of the taper and top-view of the device; (b) Cross section of the taper tip; (c) Plot of mode transformation between the SOI and III-V waveguide.

3. Static characteristics

The chip is mounted on a temperature-controlled stage set to 20 °C. We use single mode fiber to couple the light from each side of the device through grating couplers. A polarization controller is used in the measurement system to couple transverse electric (TE) polarized light into the SOA. The series resistance of the device is 12.5 Ω. The SOA gain characteristics shown in Fig. 2 represents the chip gain after compensating for the fiber-to-chip coupling loss (−7 dB for each port, which is acquired by fitting the measured loss of waveguides with different lengths). Figure 2(a) shows the gain as a function of injected current at a wavelength of 1550 nm, for different optical input power levels. The gain of the SOA as a function of input power for different wavelengths is shown in Fig. 2(b) for a bias current of 80 mA. Figure 3(a) shows the amplified spontaneous emission (ASE) spectrum of the hybrid III-V/Si SOA as a function of bias current measured using an Anritsu MS9740A optical spectrum analyzer with 0.03 nm resolution bandwidth. The ripple in the ASE spectrum is hardly visible, indicating that the reflection disturbs very little the travelling wave inside the SOA. The estimated facet reflection of the SOA is below 10^{-4}, which corresponds to a ripple of 0.2 dB according to our calculation based on transfer matrix method, as shown in Fig. 3(b).
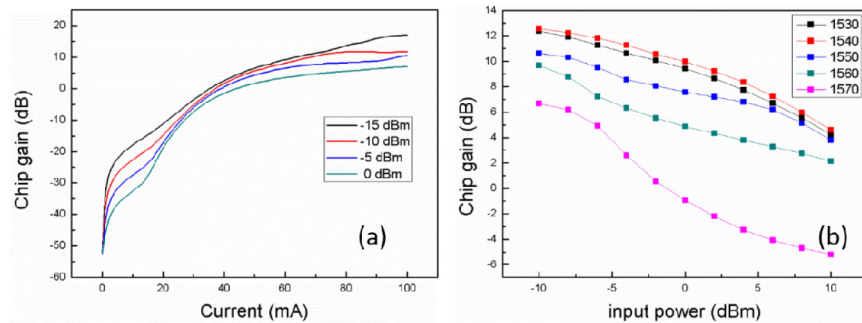

Fig. 2. (a) Chip gain vs. current at different input optical power (1550 nm wavelength); (b) Net gain variation with input optical power at different wavelengths (80 mA bias current).
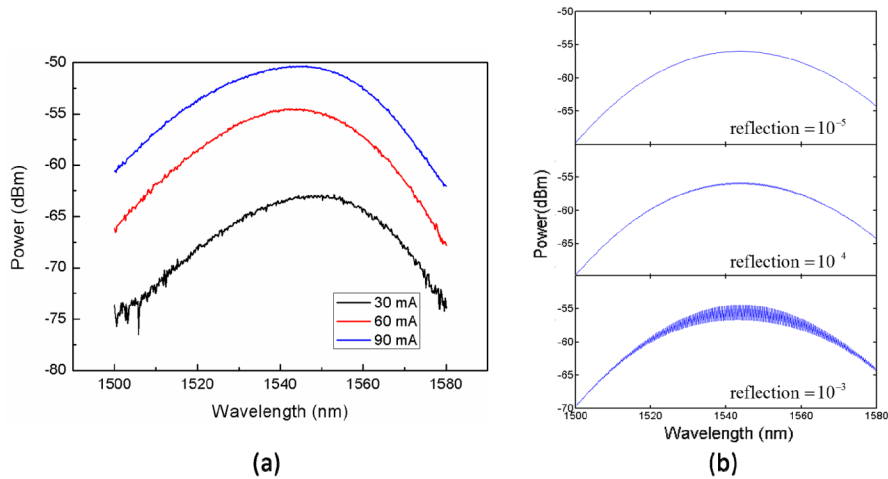

Fig. 3. (a) Measured ASE spectra as a function of injected current; (b) Calculated ASE spectrum at 60 mA with faced reflection varying from 10^{-5}, via 10^{-4}, to 10^{-3}.

4. Dynamic characteristics

AOWC using cross-gain modulation in the heterogeneously integrated SOA is achieved by using the setup shown in Fig. 4. Two tunable lasers are used for the signal and probe beams, respectively. A pulse-pattern generator (PPG) generates a data stream in 2^{31}-1 NRZ pseudorandom binary sequence (PRBS) format, which is applied to the external modulator of tunable laser 1. The optical signal at λ_1 is coupled into the SOA through a circulator. The CW light at wavelength λ_2 is coupled into the SOA in the opposite direction. At the third port of circulator, we obtain the signal at λ_2 after cross-gain modulation inside the SOA. An optical bandpass filter with a narrow bandwidth of 0.2 nm (25 GHz) is adopted to filter out the amplified spontaneous emission (ASE) noise. In order to improve the eye diagram, it is important to accurately adjust the center wavelength of the filter. During XGM, the probe light experiences a red chirp at the falling edge. A slightly blue-shifted OBF can therefore attenuate the power of the probe light. Afterwards the chirp of the probe light quickly turns to positive and reaches a maximum value. Then, the chirp decreases to zero slowly together with the gain recovery. The blue-shifted OBF can balance the power between the blue-chirped part and none-chirped part during gain recovery. As a result, the net power at the OBF output is approximately constant. In this way, we can obtain a much faster amplitude recovery time rather than the gain recovery time [21].
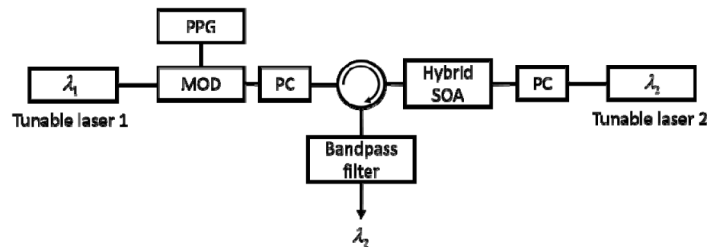

Fig. 4. Schematic of the measurement setup for AOWC. PPG: pulse-pattern generator; MOD: modulator; PC: polarization controller.

The SOA is biased at 85 mA. The average power of the optical signal λ_1 at 1545 nm that is injected into the SOA is −6.5 dBm. Because the insertion loss of the fiber-to-chip grating coupler changes with wavelength, the net input power at 1560 nm is 2 dB higher than at 1545 nm, namely −4.5 dBm. The net power of the CW light at λ_2 (at 1553 nm) is 0.5 dBm.
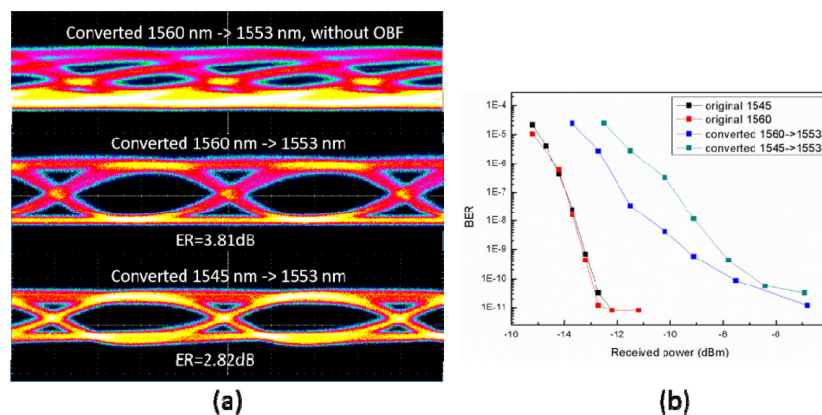

Fig. 5. (a) Eye diagram of converted signals at 12.5 Gb/s, (b) BER results.

The first eye diagram in Fig. 5(a) shows the converted signal at 12.5 Gb/s for conversion from 1560 nm to 1553 nm without an OBF. We can see that the eye diagram is almost closed

due to the large gain recovery time. With an OBF, we can improve the signal quality. In Fig. 5(a), the remaining two eye diagrams are the converted signals at 12.5 Gb/s from 1560 nm down to 1553 nm and from 1545 nm up to 1553nm with an OBF. Eye diagrams were measured using a Tektronix DSA 8300 sampling oscilloscope. The input optical signal had an extinction ratio (ER) of 9.8 dB. For wavelength down-conversion from 1560 nm to 1553 nm, we obtain a clear eye diagram with an ER of 3.81 dB. For wavelength up-conversion from 1545 nm to 1553 nm, the ER is 2.82 dB. In Fig. 6(b), we show the BER results at 12.5 Gb/s. Error-free operation (BER 10^{-9}) is obtained. In this particular experiment, the power penalty of the down-converted signal is about 1 dB smaller than that of the up-converted signal at a bit error rate of 10^{-9}.

The 40 Gb/s performance is shown in Fig. 6(a). The NRZ PRBS sequence length is 2^7-1. Because of the limitation of our measurement equipment, the original optical signal is of limited quality. Also, as the 40 Gb/s receiver used in the experiment was AC-coupled, no extinction ratio measurement could be done. The BER measurements are shown in Fig. 6(b). A power penalty less than 3 dB is obtained at a bit error rate below 10^{-5}. These results are promising to achieve error-free AOWC of 40 Gb/s NRZ data over a 15 nm wavelength span. By increasing the device active length, the number of quantum well and injection current, the SOA's gain will increase and gain recover time will reduce, enabling 40 Gbit/s error-free operation.
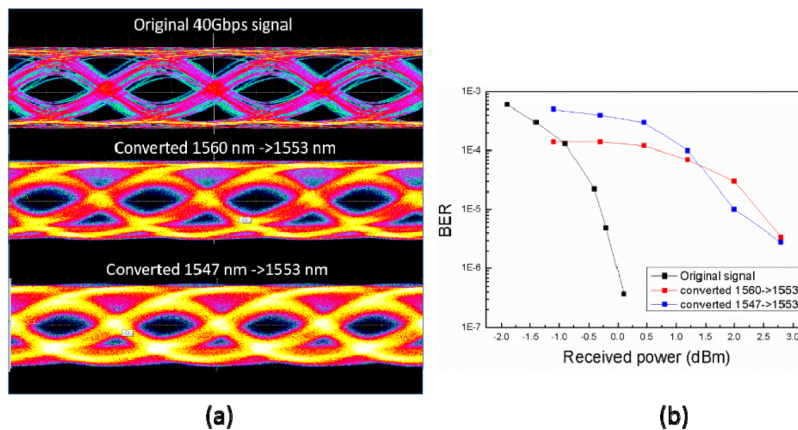

Fig. 6. (a) Eye diagram of converted signals at 40 Gb/s, (b) BER results.

5. Conclusion

All-optical wavelength conversion based on a single InP-on-SOI heterogeneously integrated SOA and optical filtering has been demonstrated at 12.5 Gb/s. The power consumption of the optical amplifier is below 250 mW, leading to an energy consumption of 6 pJ/bit at 40 Gb/s for the converter. The CW power and signal power are only 0.5 dBm and −6.5 dBm, respectively. The low power level of the CW signal enables the co-integration of the laser source on the same waveguide platform. The wavelength conversion bandwidth can be further improved by increasing the active length of the SOA and modifying the quantum well structures for higher confinement factor and differential gain coefficient. It can also be improved by co-directional propagation of signal and probe [22]. The required filter functions can be realized using silicon photonic filters integrated on the same waveguide platform.

Funding